Diagnosis of Broken Bar Fault in Three-Phase Induction Motors Using Fibre Bragg Grating Strain Sensors Assisted by an Algorithm

Rafael Cavalcanti*‡, Uilian José Dreyer¶,
Everton Luiz de Aguiar‡, Jean Carlos Cardozo da Silva§,
Kleiton Morais Sousa‡, André Mendes*†
* Research Centre in Digitalization and Intelligent Robotics (CeDRI), Instituto Politécnico de Bragança,
Campus de Santa Apolónia, 5300-253 Bragança, Portugal,
Email: a.chaves@ipb.pt
† Laboratório Associado para a Sustentabilidade e Tecnologia em Regiões de Montanha (SusTEC),
Instituto Politécnico de Bragança, Campus de Santa Apolónia, 5300-253 Bragança, Portugal
§ Programa de Pós-Graduação em Engenharia Elétrica e Informática Industrial, UTFPR, Curitiba, Brazil
Email: jeanccs@utfpr.edu.br
‡ Programa de Pós-Graduação em Engenharia Elétrica e da Computação, UTFPR, Pato Branco, Brazil
Email: kleitonsousa@utfpr.edu.br
¶ Programa de Pós-Graduação em Sistemas de Energia, UTFPR, Curitiba, Brazil
Email: uiliandreyer@utfpr.edu.br

2025 SBMO/IEEE MTT-S International Microwave and Optoelectronics Conference (IMOC) | 979-8-3503-9275-3/25/$31.00 ©2025 IEEE | DOI: 10.1109/IMOC65414.2025.11365738

***Abstract*—This study developed an algorithm running on the cloud that makes data process and diagnoses broken rotor bar faults in three-phase induction motors (TIMs), by analyzing stator dynamic deformation using fibre Bragg gratings (FBGs) as sensors. This method can diagnose mechanical faults (misalignment, imbalance) and electrical faults (fractures or cracks in rotor rings or bars). FBG-based sensors were used due to their high multiplexing capability, electromagnetic radiation immunity, and long-distance operation. Tests were conducted on a small-scale induction motor (3 HP) coupled to a generator to simulate load and the generator supplied by the grid. Were used 1 healthy rotor and one rotor with a broken bar fault running at two load conditions, 75% and 100%. The algorithm successfully identified broken bar faults in two frequency regions: around the mechanical rotational frequency of the rotor 28.06 Hz and 31.014 Hz operating at 75%; 25.325 Hz and 32.995 Hz operating at 100% and approximately twice the electrical frequency supply, 118.455 Hz and 123.942 Hz operating at 75%; 117.237 Hz and 124.683 Hz operating at 100%. The system showed high sensitivity, a good signal-to-noise ratio, and advantages over conventional methods for detecting broken bar faults in induction motors**

***Index Terms*—Algorithm, Dynamic strain, Fiber Bragg gratings, Induction motor, Rotor broken bar fault.**

I. Introduction

Three-phase induction motors (TIMs) are crucial in industrial applications due to their efficiency, robustness, and low maintenance. They account for nearly 50% of global electricity consumption, with performance enhanced by power electronics and digital control advancements [1], [2].

Despite their reliability, TIMs suffer from failures, primarily in bearings (40–50%), stators (30–40%), and rotors (5–10%) [3], [4]. These failures result from aging, contamination, or manufacturing defects, leading to costly downtime and safety risks in critical sectors [5], [6].

Fault detection relies on monitoring stator current, vibration, and temperature. Broken rotor bars cause vibrations, noise, and efficiency losses, accelerating motor aging [7]. While Motor Current Signature Analysis (MCSA) is widely used, it faces challenges from voltage harmonics and false diagnostics [8], [9].

Fiber Bragg Gratings (FBGs) offer advantages, including EMI immunity, compact size, and multiplexing capability for measuring multiple parameters [10], [11]. Previous studies used FBGs to detect rotor faults via stator deformation but required manual analysis [12].

This work proposes an automated, cloud-based FBG system for rotor fault detection, eliminating manual signal processing. The algorithm enhances accuracy by filtering inconclusive data and performing real-time analytical calculations, improving diagnostic reliability and accessibility.

II. Materials and Methods

A. Fabrication and Installation of Fiber Bragg Gratings (FBGs)

The fabrication of the FBGs was carried out at the Photonics Laboratory of the Federal University of Technology - Parana. Four FBGs were successfully written on a single-mode optical fibre using a phase mask method with a $248nm$ Excimer laser. Each FBG had a high reflectivity exceeding 70% and was carefully designed with Bragg wavelengths at $1531nm$, $1536nm$, $1540nm$, and $1560nm$, having a bandwidth of $0.3nm$. To ensure accurate strain measurements, the FBG strain sensors were pre-tractioned, enabling the detection of both positive and negative strains, with a strain sensitivity of $1.2pm/\mu\varepsilon$.

To measure dynamic strain, the FBGs were symmetrically installed in the motor stator with a $90°$ phase difference between each sensor. The installation process involved thorough cleaning of the stator teeth using acetone-soaked cotton to ensure a suitable bonding surface. The FBGs were then placed between consecutive stator teeth in a symmetrical and evenly

spaced arrangement. Cyanoacrylate glue was used for bonding, and an estimated tension of 0.1nm was maintained on one end of each FBG. The installation process was meticulously repeated for the remaining FBGs, ensuring a consistent approach throughout.

By following this careful installation process, the FBG deformation sensors were securely and accurately installed on the stator in Figure 1, facilitating precise strain measurement and analysis.

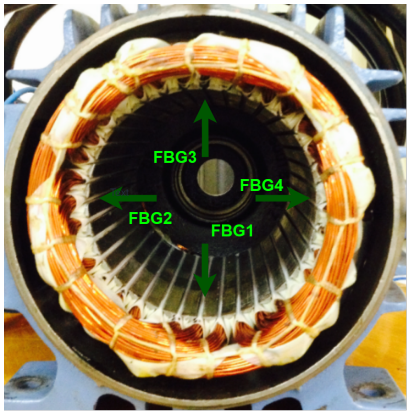

Fig. 1. The four FBGs are separated by an angle of 90°, between the stator teeth.

B. Strain frequency components of a motor running with rotor broken bar

In an induction motor, balanced three-phase currents create a rotating magnetic field in the air gap, matching its synchronous angular velocity, ω_s. This rotating field induces an electrical current in the rotor bars, which generates another magnetic field aligned with the rotor's rotation, with an angular velocity of $s\omega_s$. The slip, denoted by s, quantifies the percentage difference between the rotor's angular velocity, ω_r, and the synchronous angular velocity, ω_s, and can be calculated using Equation 1:

$$s = \frac{\omega_s - \omega_r}{\omega_s}. \tag{1}$$

Considering a healthy rotor, $\omega_r = \omega_s(1-s)$ represents the rotor angular velocity. Asymmetries in the rotor lead to the formation of a counter-rotating magnetic field with the same magnitude but in the opposite direction. This counter-rotating field has an angular velocity of $s\omega_s$ when referred to the rotor and an angular velocity of $(1-s)\omega_s - \omega_s = (1-2s)\omega_s$ when referred to the stator.

Is crucial to emphasize that, under normal operating conditions, the amplitude of the upper-frequency band is typically higher than that of the lower-frequency band. However, this pattern can change when the inertia of the motor-load assembly reaches or surpasses fifteen times the motor's inertia. In such scenarios, the amplitude relationship between the upper and lower frequency bands may be altered, potentially leading to different harmonic behaviour in the motor system. This phenomenon deserves close attention as it can significantly impact the overall performance and stability of the motor system under specific operating conditions [13], [14].

When a broken bar exists in the rotor of the motor, it induces oscillations in the motor's speed at a frequency of two times the supply frequency times the slip $2sf$. These oscillations modulate the rotation frequency, f_r, resulting in the appearance of sidebands around f_r in the stator vibration spectrum. The sidebands can be identified by values of $f_r \pm 2ksf$, and their magnitudes depend on the extent of speed oscillations and the asymmetry of the rotor.

To detect a broken bar fault, it is advisable to analyze the frequency range surrounding the motor's rotation frequency in the spectrum. By examining the presence and magnitude of frequency components expressed as f_{bq} in Equation 2 [12], [15]:

$$f_{bq} = f_r \pm 2ksf. \tag{2}$$

Among the frequency components provided by Equation 2 and shown in Figure 2, those with frequencies of $f_r \pm 2sf$ exhibit the highest magnitudes. Specifically, when $k = 1$, observing these frequency components enables more accurate identification of the rotor fault.

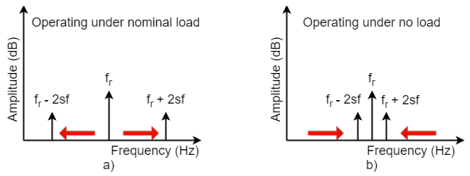

Fig. 2. Stator strain frequency spectrum of focusing on the mechanical rotating component under bar faults operating conditions.

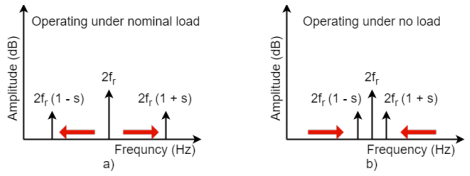

Fig. 3. Stator strain frequency spectrum of focusing on two times the supply frequency component under bar faults operating conditions.

The twice-the-power supply frequency component holds significant importance in the vibration spectrum of an induction motor. This frequency emerges due to the peak attractive force between the stator and rotor of the machine when the rotor's magnetizing current reaches its maximum positive or negative value. Consequently, at each positive or negative peak of the power supply, the attraction force between the rotor and stator intensifies. The relative position of sidebands, Figure 2, in the spectrum of a rotor broken bar for the region around its rotation frequency f_r, for $k = 1$, when: a) is the motor operating at rated load and b) image is the motor operating at no-load.

C. Experimental Setup

In this experimental setup, we focus on a 3 hp 4 pole motor crafted by WEG, which functions at 220 V and employs a delta-connected configuration. Our investigation subjects the motor to tests utilizing two distinct rotors: one representing a standard operational state (devoid of broken bars), and the other intentionally engineered to simulate a rotor fault.

For data acquisition, Fiber Bragg Gratings (FBGs) are enlisted. The task of reading these FBGs falls to a DI-410 optical sensing interrogator, while the data capture itself is executed through the catmanEASY software, a product of HBM's innovation. Notably, the DI-410 interrogator boasts the capacity to engage with four input channels, enabling simultaneous readings from multiple multiplexed sensors all integrated into a single optical fibre.

To delve deeper into specifics, data acquisition transpires at a frequency of $1kHz$, ensuring precision down to $1pm$. Such meticulous data gathering within this sophisticated experimental configuration empowers us to conduct thorough analyses of the motor's performance and behaviour across diverse rotor conditions.

The experimental setup involves the utilization of a synchronous generator, supplied by the grid, to apply various loads to the induction motor. To do that the axle of the generator is coupled to the TIM and load cells are employed to precisely measure the load torque during the experiments in the generator, as depicted in Figure 4.

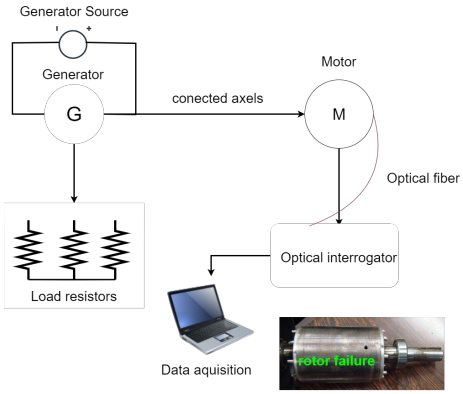

Fig. 4. Setup used in the experimental arrangement.

Two distinct testing scenarios were conducted: one utilizing the grid power supply, and the other using a frequency inverter. Each motor was subjected to tow load conditions: 75% load, and 100% load. Throughout the tests, the motors operated at a frequency of 60Hz, which is commonly encountered in industrial settings. This deliberate choice aimed to simulate a real-world operating environment, including the presence of noise, harmonics, and other disturbances. However, it is crucial to acknowledge that these conditions pose a greater challenge for the accurate diagnosis of potential faults [3].

D. Algorithm Development and Data Analysis

In this study, a Python algorithm was developed for data analysis and processing from the optical interrogator. Unlike the traditional approach that relies on catmanEASY software, this algorithm was executed on the Google Colaboratory platform, enabling cloud-based accessibility from anywhere. Leveraging the APreader library, the algorithm reads and opens files containing measurement data, granting access to all channels, sensors, time, and measurement characteristics.

The data extraction process from the sensors comprises two critical steps. Firstly, the signal is acquired from the optical interrogator using a notebook. Subsequently, the collected data is opened and analyzed through the software's filtering and analysis mode for necessary adjustments. To facilitate this analysis, the **APRead** library (Catman AP Reader) is employed, enabling the detailed scrutiny of raw data and providing valuable insights into measurements.

Upon accessing the measurements, signal processing was initiated, including the application of Fast Fourier Transform (FFT) using the **numpy.py** library to analyze Frequency (Hz) vs. Power (dB) data. This transformed data, available in graphical and list formats, becomes amenable to mathematical analysis, particularly in diagnosing rotor faults through dynamic deformation analysis.

Peak identification and data analysis follow a specific strategy. The first step involves verifying the accuracy of the measurement, distinguishing it from noise or deviations from expected values. Next, slip calculation is performed by determining the main components f_r and $2f_r$. Subsequently, additional peaks alongside the main components are examined. The presence of sidebands corresponding to expected values [12], along with the alignment of average numbers with calculated values, allows for the assumption of a rotor bar fault.

This virtual environment enables the identification of key components pivotal in rotor fault detection. The analysis conducted in this setting holds a critical role in fault detection, contributing to an enhanced comprehension of data and facilitating the effective identification of rotor faults.

III. RESULTS AND DISCUSSIONS

Figures 5, 6, 7 present one example of the frequency spectra obtained for the TIM under investigation, operating at a power supply frequency of 60 Hz, with a rotor fault and in a healthy condition, considering two different loads. Remarkably, the frequency spectra for both loads (with fault) reveal similar frequency components associated with mechanical and electromagnetic forces within the motor. The primary distinction among these spectra lies in the sidebands' frequencies and power levels. These components are directly linked to the rotational speed of the axis, which decreases as the load applied to the motor increases, with or without a fault.

In the first dataset from Table I, the motor operates with a healthy rotor at 100% load and a slip of 4.85%. The main component observed is $30Hz$ with a distinct frequency from the centre. In the second dataset, the rotor has a fault and

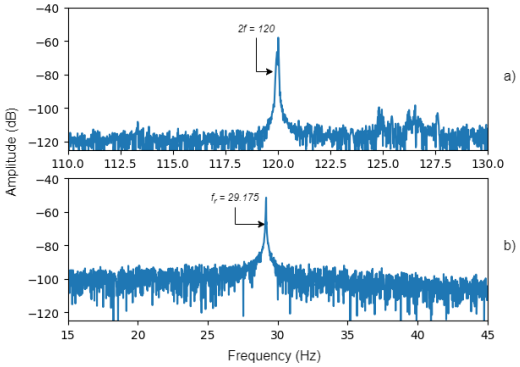

Fig. 5. Stator strain frequency spectrum: healthy rotor bar near twice the supply frequency (a) and the rotating frequency (b). The motor operates on a *60 Hz* grid and at *100%* load conditions.

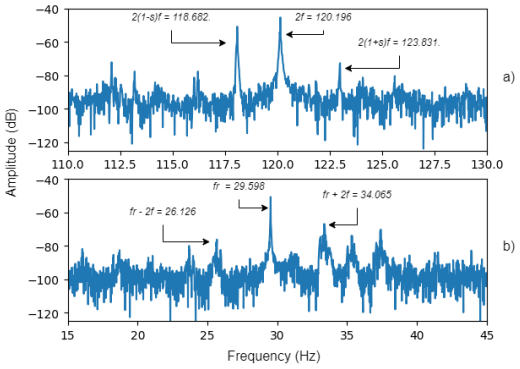

Fig. 6. Stator strain frequency spectrum for the broken rotor bar: near twice the supply frequency (a) and the rotating frequency (b). The motor operates on a *60 Hz* grid and at *75%* load conditions.

operates at 75% of the nominal load, with a slip of 1.52. The sidebands appear in the two principal components: $f_r - 2f = 28.06Hz$, $f_r + sf = 31.014Hz$, $2(1-s)f = 118.455Hz$, $2(1+s)f = 123.942Hz$. The last dataset involves the TIM operating with a rotor fault at 100% of the nominal load, with a slip of 3.157. The sidebands are observed in the two principal components: $f_r - 2f = 25.325Hz$, $f_r + sf = 32.995Hz$, $2(1-s)f = 117.237Hz$, $2(1+s)f = 124.683Hz$. The analysis considered all the FBG strain sensors and collected data, and the diagnoses matched the results presented in [12], ensuring that all the data were reliable.

Table I displays the frequency components present in each power spectrum and the correlated sidebands shown in the Figures. The main components at $120Hz$ and $30Hz$ are considered. Additionally, Table II provides information on the number of disregarded data points during the analysis.

For the initial set of tests, conducted with the grid as the power source, we applied the developed algorithm to analyze 4 peaks. Our approach involved identifying the highest power peak within the expected range calculated analytically and excluding readings that appeared inconclusive due to data acquisition errors. To ensure accuracy, the algorithm directly compiled the extracted data and applied a filter to remove

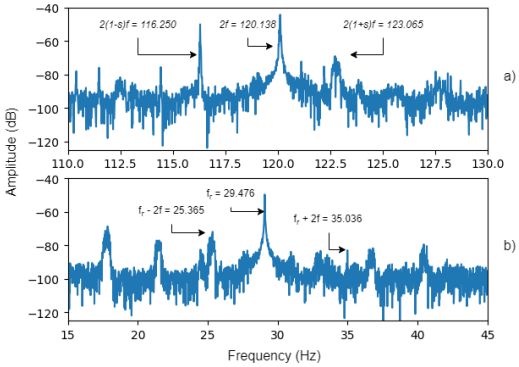

Fig. 7. Stator strain frequency spectrum for the broken rotor bar: near twice the supply frequency (a) and the rotating frequency (b). The motor operates on a *60 Hz* grid and at *100%* load conditions.

TABLE I
FREQUENCY COMPONENTS OF THE TIM RELATED TO FAULTS AND PRINCIPAL PEAKS WERE ANALYZED FOR THE MOTOR OPERATING WITH A LOAD SUPPLIED BY THE GRID.

Dataset	Slip(%)	Principal component(Hz)	Sidbands(Hz)
Healthy 100%	2.75 2.75	29.175 120.005	- -
Fault 75%	1.52 1.52	29.541 120.138	31.014 - 28.060 123.942 - 118.455
Fault 100%	3.157 3.157	29.070 119.929	32.995 - 25.325 117.237 - 124.683

inconclusive data lacking peaks corresponding to the main components f_r and $2f$.

However, relying solely on the power of the main components led to several failures in detecting faults. To address this, we considered the presence of sidebands and verified their positioning to confirm their authenticity. Using the data identified as peaks by the algorithm, we carefully analyzed all readings deemed correct and calculated their average peak values. This step allowed us to determine whether the values fell within the margin of analytical verification.

TABLE II
NUMBER OF DISCARDED DATASET

Dataset	30Hz Component (Hz)	120Hz Component (hz)
Healthy 100%	0	20
Fault 75%	1	12
Fault 100%	1	20

The strain spectrum of the stator is primarily affected by the electromagnetic forces within the machine. Additionally, the region around 30 Hz is more susceptible to mechanical forces like mechanical speed or load imbalances. When the slip values are lower, the frequency components resulting from broken bar failures tend to approach the fundamental frequencies, making it more challenging to identify the fault, mainly when the motor operates at low loads. However, we successfully identified the broken bar fault in both spectral regions analyzed, even under the two load-tested conditions.

IV. Conclusions

In this study, FBG strain sensors were employed for the detection of broken rotor bars in the TIM. Tests were conducted on both healthy and faulty rotors, ensuring isolated analysis without interference from other mechanical parameters. The motor was operated under different load conditions using a power grid and generator supplies. FBG proved effective in measuring dynamic deformation and detecting faults, with main components at 120 Hz and 30 Hz playing crucial roles in fault identification. The study emphasizes the significance of considering both the intensity and positioning of main power components and the presence of sidebands in fault detection.

The dynamic deformation signals were pre-processed using FFT and the **APreader** library, and a logical function was applied to filter relevant information for the analysis. The results indicated that the algorithm successfully detected TIM rotor faults based on motor deformation, offering an advantage over conventional software. The instrumentation used was non-invasive and easily accessible, enhancing the authenticity of the rotor status assessment. The main contribution lies in the innovative application of a cloud-based algorithm for efficient fault detection in MIT rotors, combining Python algorithms with FBG measurements.

This work presents a novel approach to fault detection in TIM rotors, harnessing the motor's dynamic deformation and advanced analysis techniques, resulting in optimized fault detection through FBG measurements.

Acknowledgements

The authors are grateful to the Foundation for Science and Technology (FCT, Portugal) for financial support through national funds FCT/MCTES (PIDDAC) to CeDRI (UIDB/05757/2020 and UIDP/05757/2020) and SusTEC (LA/P/0007/2021) and the Multi-User Photonics Facility—Federal University of Technology – Paraná, Curitiba (UTFPR - CT). This study was financed in part by the Coordenação de Aperfeiçoamento de Pessoal de Nível Superior - Brasil (CAPES) - Finance Code 001", of Conselho Nacional de Desenvolvimento Científico e Tecnológico (CNPq), from Fundação Araucária (FA) and from Financiadora de Estudos e Projetos (FINEP).

References

[1] P. C. Krause, O. Wasynczuk, S. D. Sudhoff, and S. Pekarek, *Analysis of electric machinery and drive systems*. Wiley Online Library, 2002, vol. 2.

[2] T. Jokinen, V. Hrabovcova, and J. Pyrhonen, *Design of rotating electrical machines*. John Wiley & Sons, 2013.

[3] S. Nandi, H. A. Toliyat, and X. Li, "Condition monitoring and fault diagnosis of electrical motors—a review," *IEEE transactions on energy conversion*, vol. 20, no. 4, pp. 719–729, 2005.

[4] A. Naha, A. K. Samanta, A. Routray, and A. K. Deb, "A method for detecting half-broken rotor bar in lightly loaded induction motors using current," *IEEE Transactions on Instrumentation and Measurement*, vol. 65, no. 7, pp. 1614–1625, 2016.

[5] J.-C. Trigeassou, *Electrical machines diagnosis*. John Wiley & Sons, 2013.

[6] R. Fiser and S. Ferkolj, "Application of a finite element method to predict damaged induction motor performance," *IEEE Transactions on Magnetics*, vol. 37, no. 5, pp. 3635–3639, 2001.

[7] H. A. Toliyat, S. Nandi, S. Choi, and H. Meshgin-Kelk, *Electric machines: modeling, condition monitoring, and fault diagnosis*. CRC press, 2012.

[8] J. A. Antonino-Daviu, M. Riera-Guasp, J. R. Folch, and M. P. M. Palomares, "Validation of a new method for the diagnosis of rotor bar failures via wavelet transform in industrial induction machines," *IEEE Transactions on Industry applications*, vol. 42, no. 4, pp. 990–996, 2006.

[9] M. Riera-Guasp, J. Pons-Llinares, F. Vedreno-Santos, J. A. Antonino-Daviu, and M. F. Cabanas, "Evaluation of the amplitudes of high-order fault related components in double bar faults," in *8th IEEE Symposium on Diagnostics for Electrical Machines, Power Electronics & Drives*. IEEE, 2011, pp. 307–315.

[10] S. Yin, P. B. Ruffin, and T. Francis, *Fiber optic sensors*. CRC press, 2017.

[11] J. Liu, "Study on multiplexing ability of identical fiber bragg gratings in a single fiber," *Chinese Journal of Aeronautics*, vol. 24, pp. 607–612, 2011.

[12] K. M. Sousa, I. B. V. da Costa, E. S. Maciel, J. E. Rocha, C. Martelli, and J. C. C. da Silva, "Broken bar fault detection in induction motor by using optical fiber strain sensors," *IEEE Sensors Journal*, vol. 17, no. 12, pp. 3669–3676, 2017.

[13] G. Bossio, C. De Angelo, C. Pezzani, J. Bossio, and G. Garcia, "Evaluation of harmonic current sidebands for broken bar diagnosis in induction motors," in *2009 IEEE International Symposium on Diagnostics for Electric Machines, Power Electronics and Drives*. IEEE, 2009, pp. 1–6.

[14] G. Didier, E. Ternisien, O. Caspary, and H. Razik, "A new approach to detect broken rotor bars in induction machines by current spectrum analysis," *Mechanical Systems and Signal Processing*, vol. 21, no. 2, pp. 1127–1142, 2007.

[15] K. M. Sousa, U. J. Dreyer, C. Martelli, and J. C. C. da Silva, "Dynamic eccentricity induced in induction motor detected by optical fiber bragg grating strain sensors," *IEEE Sensors Journal*, vol. 16, no. 12, pp. 4786–4792, 2016.